

## MATERIALS AND INTERFACES

# Effect of Poly(aspartic acid) on the Removal Rates of Brushite Deposits from Stainless Steel Tubing in Turbulent Flow

Felicia Littlejohn<sup>†</sup> and Christine S. Grant\*

Department of Chemical Engineering, North Carolina State University, Raleigh, North Carolina 27695-7905

Yu Ling Wong and A. Eduardo Sáez

Department of Chemical and Environmental Engineering, University of Arizona, Tucson, Arizona 85721

This research investigates the effect of poly(aspartic acid) (PASP) and its sodium salt on the removal of brushite (dicalcium phosphate dihydrate, DCPD) deposits from stainless steel tubing in turbulent flows. In the absence of PASP, DCPD removal is dominated by the abrasion of solid particles from the deposit by fluid shear and is influenced by the kinetics of the interfacial dissolution process. The presence of PASP promotes DCPD removal for pHs between 4 and 10, with an optimum enhancement at pH 5. A decrease in the sensitivity of the removal rate to shear forces indicates that PASP inhibits solids detachment from the deposit for pH < 5. At higher pHs, PASP appears to reduce the shear stress required to remove particles from the deposit. A model for the interfacial dissolution process that includes mass transfer, adsorption equilibria, and the kinetics of acid dissolution and surface complexation is used to explain the trends of the experimental data on removal rates.

### Introduction

Sequestering agents are compounds that form complexes with metal ions. Sequestrants bind to cations, such as calcium, to form ion complexes. A chelating agent is a type of sequesterant that forms complexes in which the cation is held within the chelate by multi-dentate ion coordination. Resonant functional groups, such as carboxylic functions, enable the complex to maintain a residual charge following complexation, so that the resulting ion pair remains soluble.

Sequestrants are primarily used in detergent formulations to control and prevent deposit formation. The deposition of minerals in industrial processing equipment is a serious problem because it may lead to obstruction of fluid flow in piping and a reduction in heat-transfer rates. The formation of calcium phosphate scales, in particular, is predominant in cooling towers because of the use of recycled water or untreated makeup water containing higher orthophosphate levels.<sup>1</sup> In dairy applications, the aqueous phase of milk is supersaturated with calcium phosphate. High-temperature processing causes precipitation of calcium phosphate because of its inverse solubility behavior. Sequestrants may be used to prevent the nucleation, growth, and precipitation of calcium phosphate crystals.

There are environmental regulatory issues associated with sequesterant selection. For example, the use of sodium tripolyphosphate (STPP) has been banned in

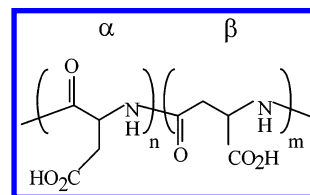


Figure 1. Chemical structure of poly(aspartic acid).

many parts of the world because its usage is associated with the eutrophication of lakes and stagnant waters.<sup>2</sup> Ethylenediaminetetraacetic acid (EDTA) is an effective sequesterant and may be used to replace STPP in some detergent formulations. However, there are concerns about EDTA usage in some applications because of its slow biodegradability and possibility of causing heavy-metal mobilization in groundwater.<sup>3,4</sup> Poly(acrylic acid) is also an effective calcium sequesterant, but it also degrades slowly.<sup>5,6</sup> Sodium citrate, on the other hand, is readily degradable and nontoxic but tends to be a less effective sequesterant. Investigators continue to seek sequestrants that are both effective and environmentally safe because they provide a feasible alternative to acid dissolution, which may cause corrosion of pipes and undesirable contamination in applications such as the dairy industry.

This research involves the study of the sodium salt of poly(aspartic acid) (PASP) (Figure 1). Poly(aspartic acid) is a promising developmental polycarboxylic sequesterant that is nontoxic, biodegradable, and water-soluble.<sup>7</sup> Sikes and Wheeler<sup>8</sup> studied the sequestering ability of polyaspartate obtained from the organic component of oyster shells. Low-cost manufacturing procedures have been developed to synthesize PASP for

\* To whom correspondence should be addressed. E-mail: grant@eos.ncsu.edu. Phone: 919-515-2317. Fax: 919-515-3465.

<sup>†</sup> Present address: E.I. duPont de Nemours and Co., Chattanooga, TN.

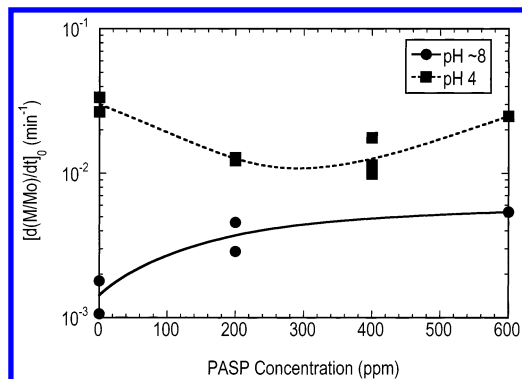


**Figure 2.** Effect of pH and poly(aspartic acid) concentration on the removal rate of HAP/DCPD deposits from stainless steel tubing in turbulent flow.<sup>11</sup> The fluid velocity was 1.2 m/s, and the experimental setup was the same as that used in the present work. Lines are smoothed fits of the data points. The normalized removal rates correspond to the beginning of the cleaning process.

commercial use.<sup>5</sup> Currently, PASP is used as a dispersant to prevent the redeposition of minerals, such as hydroxyapatite (HAP:  $\text{Ca}_5(\text{PO}_4)_3\text{OH}$ ),<sup>5</sup> an inhibitor of the salt crystallization and precipitation,<sup>9</sup> a water softener, and a corrosion inhibitor.<sup>10</sup>

Previous research by our group<sup>11</sup> on cleaning of deposits from the inner wall of stainless steel pipes in turbulent flow has shown that, under alkaline conditions, PASP enhances the removal of calcium phosphate deposits consisting of a mixture of HAP and brushite (calcium hydrogen phosphate dihydrate or dicalcium phosphate dihydrate, DCPD;  $\text{CaHPO}_4 \cdot 2\text{H}_2\text{O}$ ). Figure 2 shows illustrative results of cleaning studies carried out at different PASP concentrations at an alkaline pH (pH 8) and an acidic pH (pH 4). The plot shows the initial cleaning rate as the mass of deposit removed per unit time at  $t = 0$ ,  $(dM/dt)_0$ , normalized by the initial total mass of the film,  $M_0$ . As shown in Figure 2, PASP facilitates calcium phosphate removal over concentrations ranging from 0 to 600 ppm at the alkaline pH. A 600 ppm PASP solution results in a removal rate that is 4 times faster than that in the absence of PASP. At a low pH (pH 4), the sequesterant inhibits removal at low concentrations (below 300 ppm). This result is analogous to findings by Christoffersen and Christoffersen,<sup>12</sup> who observed that low concentrations of citrate ions inhibit HAP dissolution under acidic conditions, while higher concentrations increased the rate of dissolution. The inhibition was believed to be caused by the adsorption of the citrate ligand to the crystal surface.

Batch dissolution experiments for the HAP/DCPD system showed that, under alkaline conditions, the total amount of calcium in solution increased in the presence of PASP, while at the same time the amount of  $\text{Ca}^{2+}$  ions decreased.<sup>11</sup> This indicates that sequestration of calcium ions by PASP represents the major driving force for the enhanced dissolution of HAP/DCPD mixed deposits at alkaline pHs.

Furthermore, we have determined that the mechanism by which the HAP/DCPD mineral is removed from the pipe surface in the absence of PASP is the dissolution of the calcium salt into the flowing solution.<sup>13</sup> Both the interfacial dissolution rates and mass transfer from the deposit to the bulk solution played a quantitative role in the process, except at very low pHs, for which dissolution was fast and mass-transfer rates were the controlling factor.

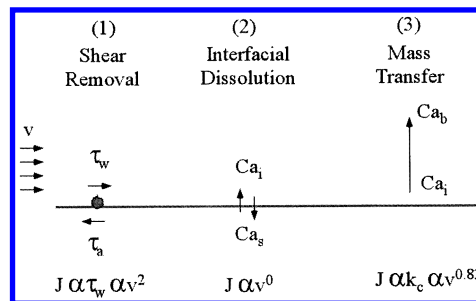


**Figure 3.** Rate-controlling mechanisms of calcium phosphate removal from surfaces: (1) Shear removal: solid particles are detached from the surface when the applied shear stress ( $\tau_w$ ) exceeds the stress of adhesion of the particle ( $\tau_a$ ). (2) Interfacial dissolution: the kinetics of adsorption/desorption processes at the interface controls the removal. (3) Mass transfer: convective mass transfer from the surface to the bulk solution controls the removal. The dependence of removal flux on fluid velocity is presented for the case in which each mechanism dominates.

Our previous studies with HAP/DCPD deposits indicate that PASP is effective in increasing removal rates under conditions for which its complexation of calcium ions becomes significant in the dissolution process (alkaline pHs and increased PASP concentrations). However, the removal of mixed HAP/DCPD deposits is kinetically controlled by a combination of surface dissolution and mass-transfer rates. It is not clear how effective the sequesterant can be when the predominant removal mechanism is the action of shear forces to detach solid particles from the deposit surface. In a previous work,<sup>13</sup> we have determined that this mechanism controls the removal of deposits of pure DCPD in the absence of sequesterants. For this reason, the main objective of this work is to determine the mechanisms by which PASP affects deposit removal of pure DCPD films at various pHs and fluid velocities. This work uses a solid scintillation technique applied in previous research by our group<sup>11,13-16</sup> to experimentally study the removal of DCPD deposits from stainless steel pipes under turbulent flow conditions in the presence of PASP. By comparing DCPD deposit removal in the presence and absence of PASP, we establish how the sequesterant affects the shear-controlled cleaning rate. We also explore how cleaning mechanisms and rates compare to those of HAP/DCPD mixed deposits measured in previous works.

## Theory

In this section we present an overview of the mechanisms responsible for calcium phosphate deposit removal from stainless steel pipes in turbulent flows. We also develop a detailed model for dissolution rates of DCPD deposits.

**Removal Mechanisms.** Calcium phosphate deposits might be removed by dissolution by chemical agents or by solids detachment under the action of shear forces. When dissolution is the prevailing mechanism, the dissolved species are transferred from the solid/liquid interface to the bulk solution by convective mass transfer. The kinetics of the removal process might depend on one or more of the following kinetic steps: the rate of shear removal, rate of interfacial dissolution, and rate of mass transfer. These are detailed in what follows and are shown schematically in Figure 3.

(1) Shear removal. The removal of deposits from pipe walls by mechanical action can be conceptualized as

resulting from the detachment of particles from the solid surface under the action of the shear stress exerted by the fluid,  $\tau_w$ . The shear stress can be represented in terms of the average velocity of the fluid in the pipe,  $v$ , by means of the Darcy friction factor,  $f$ , as follows:

$$\tau_w = \frac{1}{8}\rho v^2 f \quad (1)$$

where  $\rho$  is the fluid density. The Darcy friction factor depends on the Reynolds number and, in turbulent flows, on the relative roughness of the pipe wall. In this case, the roughness is that of the exposed surface of the mineral deposit. Typically, these deposits have a higher relative roughness than commercial pipes.<sup>11</sup> If the Reynolds number is high enough, the friction factor becomes insensitive to the value of the Reynolds number and the shear stress becomes proportional to  $v^2$ .

The removal of a specific particle from the mineral surface will occur when the shear stress exceeds a specific threshold ( $\tau_a$ ) that represents the stress that the particle can withstand while remaining attached to the surface. At a given time, all particles for which  $\tau_w \geq \tau_a$  will be removed from the surface. Because of the irregular morphology of the deposit surface,<sup>11</sup> one can speculate that there will be a distribution of particles with different threshold stresses and that this distribution might change with time as mineral dissolution changes the local morphology of the surface. Therefore, the rate of deposit removal would be a complex function of the surface morphology, and an accurate quantification of the removal rates by this mechanism would require a knowledge of the threshold stress distribution and its evolution as removal proceeds. However, for a wide distribution of threshold stresses, it is reasonable to expect that the removal flux ( $J$ , moles of deposit removed per unit time and surface area) follows the same scaling with fluid velocity as the shear stress, i.e.,  $J \propto v^2$ . This behavior has been observed in the removal of liquefied films from solid surfaces.<sup>17</sup> However, the actual force exerted on particles protruding from the film might exhibit a more pronounced velocity dependence because lift forces due to turbulent bursts close to a solid surface have been determined to be proportional to the third power of the average velocity.<sup>18</sup> In a previous work,<sup>15</sup> we determined that removal rates of DCPD deposits from pipe walls in turbulent flow over a wide range of pHs (2–10), in the absence of sequestering agents, followed a scaling  $J \propto v^{2.6}$ , which suggests that shear forces were the most important mechanism for deposit removal.

(2) Interfacial dissolution. Dissolution reactions occur at the solid–liquid interface. The process of interfacial dissolution will depend on the kinetics of such reactions, as well as the rate of adsorption and desorption of reactants and products, for reactions that occur on the surface. We analyze in detail the mechanism of interfacial dissolution of DCPD below. At this point, we only mention that, if interfacial dissolution is the rate-controlling step, then we would expect the removal rate to be independent of the fluid velocity.

(3) Convective mass transfer. The transport of dissolved species from the interface to the bulk solution occurs by convective mass transfer. If interfacial dissolution is fast and there is no particle detachment by shear forces, the removal flux is controlled by the rate of mass transfer, given by

$$J = k_m(C_i - C_b) \quad (2)$$

where  $C_i$  and  $C_b$  are the interfacial and bulk concentrations of the dissolved species, respectively, and  $k_m$  is the convective mass-transfer coefficient. For turbulent flow in a pipe, the mass-transfer coefficient can be obtained from the empirical correlation<sup>19</sup>

$$Sh = 0.023 Re^{0.83} Sc^{1/3} \quad (3)$$

where the Sherwood, Reynolds, and Schmidt numbers are defined as follows:  $Sh = k_m D/D_m$ ,  $Re = \rho v D/\mu$ , and  $Sc = \mu/\rho D_m$ , where  $D$  is the pipe internal diameter,  $\rho$  and  $\mu$  are the fluid density and viscosity, respectively, and  $D_m$  is the diffusivity of the dissolved species in the fluid. Substitution of the mass-transfer coefficient from eq 3 into eq 2 indicates that  $J \propto v^{0.83}$ .

Each of the three removal mechanisms described above yields a removal flux that has a different dependence on velocity. By measuring the flux as a function of velocity, we can ascertain which mechanisms play a role in a specific case. For example, for HAP/DCPD mixed deposits, we have determined that the flux follows the scaling  $J \propto v^\beta$ , where  $\beta$  varies from values close to 0.8 at very low pHs (below 2) to under 0.3 at high pHs (above 8).<sup>13</sup> This indicates that, as the pH is progressively increased, the removal mechanism changes from a mass-transfer control to a mixed interfacial dissolution/mass-transfer control.

**Dissolution Model.** In this section, we present a mathematical model that considers both interfacial dissolution and convective mass transfer as mechanisms participating in the removal of DCPD deposits from the inner surface of tubes under turbulent flow conditions. The model is applicable to the dissolution of DCPD into pH-controlled aqueous buffers in the absence of PASP and to the dissolution in the presence of PASP.

The dissolution of calcium phosphate into the liquid will be modeled as occurring through reversible chemical reactions with elementary kinetics. We will assume that the solid surface can be divided into two types of sites: The first type contains adsorbed polyaspartate species that directly participate in the dissolution of the deposit. The second type of site is bare of polyaspartate, and calcium phosphate dissolves directly into the liquid. The fractional surface covered by adsorbed PASP species is represented by  $\theta$ . We will assume that this fractional coverage follows the Langmuir adsorption isotherm

$$\theta = \frac{K_L C_{\text{PASP},T}}{1 + K_L C_{\text{PASP},T}} \quad (4)$$

where  $K_L$  is the adsorption equilibrium constant and  $C_{\text{PASP},T}$  is the total concentration of ionic polyaspartate species in solution at the solid–liquid interface. We will assume that the adsorption of PASP species is not a kinetically controlling process, so that the isotherm (4) applies at all times.

Poly(aspartic acid) in solution hydrolyzes because of the carboxylic acid groups present along the PASP chain (Figure 1). The quantification of the hydrolysis reactions on a molar basis is complicated by the relatively high molecular weight of the dissolved PASP. However, Silverman et al.<sup>10</sup> successfully fitted poly(aspartic acid) titration curves to dissociation reactions involving chains that could release up to four protons. According to this, if  $H_4\text{PASP}$  is the uncharged poly(aspartic acid) molecule,

then considering the species  $H_{4-m}PASP^{m-}$  for  $m = 0-4$  in solution is enough to represent the acid–base equilibrium in the polyaspartate system. We will adopt this model in the present work. According to this, the ionic PASP species in solution that can be adsorbed on the solid surface have the following total concentration:

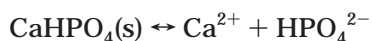
$$C_{PASP,T} = \sum_{m=1}^4 [H_{4-m}PASP^{m-}]_{(i)} \quad (5)$$

where the subscript (i) denotes interfacial concentration in the liquid.

The total flux of calcium that dissolves into the liquid phase will be represented as

$$J = \theta J_P + (1 - \theta) J_{NP} \quad (6)$$

where  $J_P$  and  $J_{NP}$  are the dissolution fluxes from the PASP-covered and PASP-free sections of the surface, respectively. The flux from the PASP-free section of the surface will be due to the direct dissolution of calcium phosphate, which will be represented by the reaction

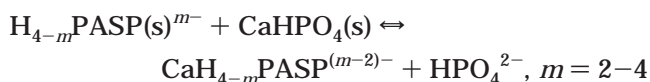


This will be treated as an elementary reaction. Because the activity of calcium phosphate in the solid phase can be considered constant, the dissolution flux can then be expressed as

$$J_{NP} = k_R - k_A [Ca^{2+}]_{(i)} [HPO_4^{2-}]_{(i)} \quad (7)$$

where  $k_R$  and  $k_A$  are kinetic rate constants for the forward and backward reactions, respectively.

The dissolution flux from the PASP-covered section of the surface will be evaluated in terms of the following reversible surface complexation reaction:



Note that we are considering that calcium complexation can occur only with PASP species whose charge is  $-2$  or more negative. The flux can be represented as

$$J_P = \sum_{m=2}^4 (k_{P1,m} - k_{P2,m} [HPO_4^{2-}]_{(i)} [CaH_{4-m}PASP^{(m-2)-}]_{(i)}) \quad (8)$$

where  $k_{P1,m}$  and  $k_{P2,m}$  are the forward and backward reaction kinetic rate constants, respectively. The activities of adsorbed PASP species on the PASP-covered sections of the surface are considered to be constant. The use of eq 8 involves six different kinetic rate constants that cannot be measured independently. For this reason, and to simplify the model, we will assume that all of the backward kinetic constants are equal, i.e.,  $k_{P2,2} = k_{P2,3} = k_{P2,4} = k_{P2}$ . Also, we define  $k_{P1} = \sum_{m=2}^4 k_{P1,m}$ , so that eq 8 can be simplified to

$$J_P = k_{P1} - k_{P2} [HPO_4^{2-}]_{(i)} \sum_{m=2}^4 [CaH_{4-m}PASP^{(m-2)-}]_{(i)} \quad (9)$$

**Table 1. Equilibrium Reactions Used in the Dissolution Model (25 °C)<sup>a</sup>**

equilibrium reactions		pK
Phosphate Equilibria		
$H^+ + H_2PO_4^- \rightleftharpoons H_3PO_4$	$K_{PE1}$	2.19
$H^+ + HPO_4^{2-} \rightleftharpoons H_2PO_4^-$	$K_{PE2}$	7.18
$H^+ + PO_4^{3-} \rightleftharpoons HPO_4^{2-}$	$K_{PE3}$	12.3
Calcium Equilibria		
$Ca^{2+} + 2H^+ + PO_4^{3-} \rightleftharpoons CaH_2PO_4^+$	$K_{CE1}$	20.95
$Ca^{2+} + H^+ + PO_4^{3-} \rightleftharpoons CaHPO_4$	$K_{CE2}$	15.09
$Ca^{2+} + PO_4^{3-} \rightleftharpoons CaPO_4^-$	$K_{CE3}$	6.46
$Ca^{2+} + 2H_2O \rightleftharpoons Ca(OH)_2 + 2H^+$	$K_{CE4}$	-27.99
$Ca^{2+} + H_2O \rightleftharpoons CaOH^+ + H^+$	$K_{CE5}$	-12.60
Water Equilibrium		
$H^+ + OH^- \rightleftharpoons H_2O$	$K_w$	-14.00
Polyaspartate Equilibria		
$H_4PASP \rightleftharpoons H^+ + H_3PASP^-$	$K_{AE1}$	2.2
$H_3PASP^- \rightleftharpoons H^+ + H_2PASP^{2-}$	$K_{AE2}$	3.6
$H_2PASP^{2-} \rightleftharpoons H^+ + HPASP^{3-}$	$K_{AE3}$	4.3
$HPASP^{3-} \rightleftharpoons H^+ + PASP^{4-}$	$K_{AE4}$	5.4
Calcium Complexation Equilibria		
$Ca^{2+} + PASP^{4-} \rightleftharpoons CaPASP^{2-}$	$K_{ME1}$	(Table 2)
$Ca^{2+} + HPASP^{3-} \rightleftharpoons CaHPASP^-$	$K_{ME2}$	
$Ca^{2+} + H_2PASP^{2-} \rightleftharpoons CaH_2PASP$	$K_{ME3}$	

<sup>a</sup> All reactions occur in the aqueous phase and are assumed to reach equilibrium instantly. Data for calcium and phosphate are from the MINEQ+ database and work by Lindsay.<sup>20</sup> Polyaspartate equilibria are from experimental data fitted to a model based on four carboxylic acid units per chain.<sup>10</sup> Equilibrium constants for calcium complexation with polyaspartate are used as adjustable parameters.

The substitution of eqs 7 and 9 into eq 6 allows us to express the total dissolution flux in terms of the interfacial concentrations of various dissolved species. In the solution at the interfacial region, we will consider that dissolved species participate in the reactions presented in Table 1. All of these reactions will be assumed to be at equilibrium; i.e., their kinetics are assumed to be much faster than the rate of dissolution. These reactions include (1) phosphate acid–base equilibrium reactions, (2) calcium acid–base and phosphate equilibrium reactions, (3) water equilibrium, (4) polyaspartate acid–base equilibrium, and (5) PASP–calcium complexation in solution. Previous work by our group<sup>11</sup> has shown that complexation of calcium ions in solution by PASP species is a fast reaction in batch dissolution processes of mixtures HAP/DCPD.

The use of the equilibrium constants in Table 1, along with stoichiometric relations, allows us to write a system of equations involving the interfacial concentrations of all of the species present in solution. We assume that the total interfacial PASP concentration is equal to the initial concentration of PASP in the cleaning solution. We also assume that the pH of the solution in the interfacial region is the original pH.

At steady state, the total dissolution flux must equal the mass-transfer flux of calcium species from the interfacial region to the bulk of the fluid. Because the solvent used in the experiments is originally calcium free and its flow rate is high compared with the dissolution flux, the bulk concentrations of calcium species are negligible. Furthermore, if the diffusivities of all dissolved calcium species are approximately the same, we can simplify eq 2 to

$$J = k_m C_{Ca,T} \quad (10)$$

where

$$C_{Ca,T} = [Ca^{2+}]_{(i)} + [CaH_2PO_4^+]_{(i)} + [CaHPO_4]_{(i)} + [CaPO_4^-]_{(i)} + [Ca(OH)_2]_{(i)} + [CaOH^+]_{(i)} + [CaPASP^{2-}]_{(i)} + [CaHPASP^-]_{(i)} + [CaH_2PASP]_{(i)} \quad (11)$$

In the application of eq 10, the mass-transfer coefficient was calculated from eq 3 using the diffusivity of  $Ca^{2+}$ .

If eq 11 is substituted into eq 10 and the dissolution flux given by eq 6 is equated to the mass-transfer flux, the model presented can be used to determine the interfacial concentrations of all of the relevant chemical species dissolved in the liquid and, in turn, the dissolution flux can be evaluated. The calculations require knowledge of the following unknown parameters: the acid dissolution kinetic constants,  $k_R$  and  $k_A$ , which can be fitted independently to dissolution experiments in the absence of PASP; the complexation equilibrium constants,  $K_{ME1}$ ,  $K_{ME2}$ , and  $K_{ME3}$ ; the Langmuir constant  $K_L$ ; and the kinetic PASP-enhanced dissolution constants  $k_{P1}$  and  $k_{P2}$ .

## Experimental Section

**Materials.** Polysuccinimide (with average molecular weights  $\bar{M}_w = 10\,000$  and  $\bar{M}_n = 2730$ ) synthesized by the acid-catalyzed thermal polycondensation of L-aspartic acid was prepared by Rohm and Haas as described by Freeman et al.<sup>7</sup> Prewashed polysuccinimide was hydrolyzed to form sodium polyaspartate by the drop-wise addition of a 50% sodium hydroxide solution to maintain a pH of about 11 until the reaction was complete. The reaction was complete when all of the polysuccinimide had completely dissolved.

A crystalline suspension of DCPD (25% solids) was obtained from the Sigma Chemical Co. The radiolabeled DCPD used for the cleaning studies (described in detail below) was obtained by irradiating a 10 g sample of DCPD suspension (Sigma Chemical Co.) in the Pulstar nuclear reactor at North Carolina State University.

**Cleaning Experiments.** The DCPD deposits were prepared for the cleaning experiments by drying a calcium phosphate slurry in a cylindrical section of tubing. The stock slurry was prepared by mixing 8 g of the DCPD suspension with 12 g of deionized water. The stock slurry was radiolabeled by the addition of  $^{32}P$ -labeled DCPD. For each experiment, a volume of 0.5 mL of radiolabeled slurry (dry weight 57.3 mg) was injected into a test cell (Figure 4). The test cell was then capped and rotated under an infrared heat lamp for 8 h at 95 °C to form a deposit. Scanning electron microscopy (SEM) micrographs show that the DCPD deposits are composed of agglomerated crystals.<sup>11</sup> X-ray diffraction showed that the DCPD deposits are essentially free of impurities and that no transformation of DCPD to other calcium phosphates occurred during the heating process.

After the test cell was placed within the experimental flow system (Figure 5), a solid scintillation detector was positioned outside of the test cell to obtain real-time measurements of the  $\beta$ -particle counts from the deposit on the inner surface of the test cell. To initiate an experiment, a solution (5 L) contained in the reservoir (20 L) is pumped through a centrifugal pump so that fluid velocities ranging from 0.8 to 2.4 m/s were obtained in the pipe and the test cell. These fluid velocities correspond to fully developed turbulent flow for  $Re$

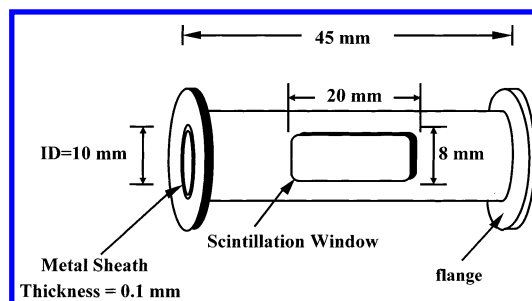


Figure 4. Diagram of the test cell.

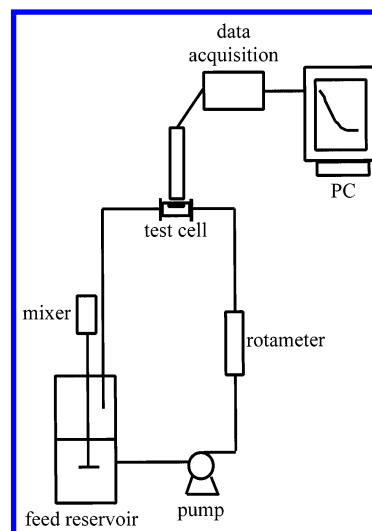


Figure 5. Schematic diagram of the flow apparatus.

ranging from 9000 to 27 000. To adjust and maintain the pH throughout the experiments, 1 M sulfuric acid or 1 M sodium hydroxide were added as needed. These chemicals were reagent-grade and were used without further purification. Automated data acquisition procedures were used to record the counts emitted from the deposit and the pH of the solution throughout the experiment. Experiments were carried out for PASP concentrations ranging from 0 to 800 ppm and pHs ranging from 2.85 to 10. Experiments were conducted at room temperature ( $25 \pm 3$  °C). The experiment concluded when the counts dropped to the background level or after a specified time period of continuous cleaning.

The data were normalized using the following equation:

$$\frac{M(t)}{M_0} = \frac{Ct(t) - B}{Ct_0 - B} \quad (12)$$

where  $M(t)$  is the mass of the deposit on the surface at time  $t$ ,  $M_0$  is the initial mass of the deposit,  $Ct(t)$  is the  $\beta$ -particle count at time  $t$ , and  $Ct_0$  is the  $\beta$ -particle count at time zero. Background counts,  $B$ , were measured by measuring the  $\beta$ -particle count in the absence of a radiolabeled deposit.

The normalized data are expressed as  $M/M_0$ , which represents the fraction of film remaining on the surface. The normalized counts were time-averaged over 5 min intervals and multiplied by the initial mass,  $M_0$ , to give the mass of the deposit remaining on the surface as a function of time,  $M(t)$ . A plot of the mass of film remaining on the surface versus time for the initial linear portion of the graph was used to determine the

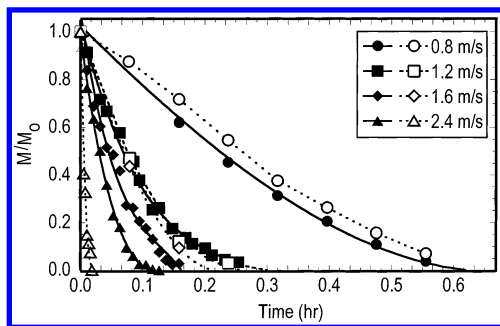


**Figure 6.** Typical cleaning curves: removal of DCPD from stainless steel tubing at pH 2.85. Solid lines and filled markers indicate DCPD cleaning studies carried out in the presence of PASP (600 ppm). Dashed lines and open markers represent DCPD cleaning studies carried out in the absence of PASP. The legend shows the average fluid velocity. The lines correspond to 5 min averages of experimental data, and the markers are selected data points used to identify the curves.

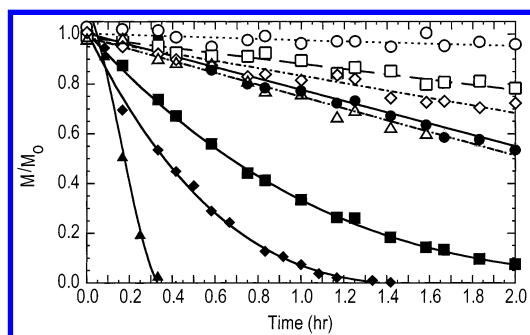


**Figure 7.** Typical cleaning curves: removal of DCPD from stainless steel tubing at pH 6. Lines, markers, and the legend are as in Figure 6.

initial removal rates. The initial cleaning rates are used in the analysis to minimize the possible effects of changes in the surface area and morphology of the deposit during the cleaning process.

Additional details about the experiments and measurement techniques have been reported elsewhere.<sup>21</sup>

## Results and Discussion

In previous research, we have shown that PASP has a significant impact on the removal rates of deposits consisting of a mixture of HAP and DCPD.<sup>11</sup> The rate of HAP/DCPD removal is limited by a slow dissolution process. At the higher pHs, we observed that the ligand promotes the deposit removal by increasing the dissolution rate. Therefore, for cleaning studies carried out at alkaline pHs, the presence of PASP significantly improved the HAP/DCPD removal rates by increasing the rate of the interfacial solubilization process. In cases of DCPD removal where shear, rather than dissolution, controls the removal rate, the effect of a polymeric sequesterant is not known. Thus, we will first seek to establish whether PASP will have any impact on the removal rate of DCPD.

To determine whether PASP affects DCPD removal rates, cleaning experiments were carried out in the experimental flow system over a wide range of pHs and fluid velocities. Representative cleaning curves are shown for pH 2.85 (Figure 6) and pH 6 (Figure 7), comparing processes in the absence of PASP with processes in which the solution has a PASP concentration of 600 ppm. Note that all of the cleaning curves are linear at low removals (i.e., high values of  $M/M_0$ ),

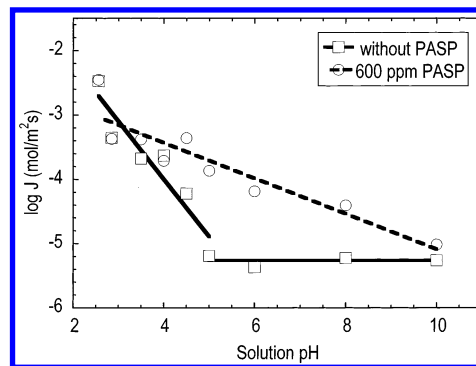


**Figure 8.** Effect of PASP on DCPD removal flux as a function of pH at  $v = 1.2$  m/s. Lines represent linear fits of the data in the corresponding ranges.

whereas toward the end of the cleaning process, they exhibit an upward curvature. This curvature has been associated with the depletion of the surface area covered by a mineral film.<sup>11,13</sup>

As explained above, the predominant removal mechanism can be determined by quantifying the effect of fluid velocity on removal rates. In the absence of PASP, shear removal is the predominant mechanism for DCPD deposits. Our results show that PASP affects the dependence of the removal rate on fluid velocity. For example, in Figure 6, the removal at a fluid velocity of 0.8 m/s in the absence of PASP is slightly slower than that using PASP, whereas the removal in the absence of PASP is appreciably faster at 2.4 m/s. This result indicates that PASP alters the ability of the DCPD deposit to withstand shear stresses.

A comparison of the data shown in Figures 6 and 7 indicates that pH also has a significant impact on the removal rates. The removal rates at pH 2.85 (Figure 6) are much higher than those measured at pH 6 (Figure 7). This is consistent with observations made previously for DCPD and HAP/DCPD cleaning data.<sup>13</sup> At pH 2.85, DCPD is more soluble than at pH 6. Therefore, based on DCPD solubility, this result is expected. The novel factor in this case is that pH not only affects the solubility of the mineral but also changes the surface charge and controls sequesterant speciation. In addition, the removal rates for cleaning studies carried out in the presence of PASP were more rapid than those in the absence of the sequesterant at all fluid velocities in Figure 7 (pH 6).

To quantify the role of pH on the effectiveness of the sequesterant, the removal flux corresponding to the initial removal rates ( $J$ ) is plotted as a function of solution pH in Figure 8 for a fixed fluid velocity. These results are compared to DCPD cleaning studies carried out without PASP. In the absence of PASP, two regimes in terms of the effect of pH are observed. At low pHs ( $\text{pH} < 5$ ), there is a significant effect of pH on the removal flux. We have postulated in a previous work<sup>13</sup> that enhanced dissolution of the mineral by direct reaction of protons with the solid at low pHs lowers the adhesion stress of mineral particles and makes them more susceptible to shear removal as pH decreases in this regime. In terms of the dissolution model developed in this work, the enhanced dissolution at low pHs can be represented as an increase in  $k_R$  as pH decreases (eq 6). At higher pHs ( $\text{pH} > 5$ ) in the absence of PASP, the removal flux becomes relatively low and independent of pH. In this regime, shear forces are solely responsible for the removal flux because acid dissolution plays a

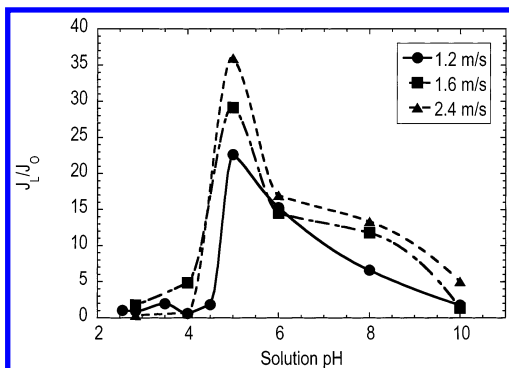


**Figure 9.** Relative improvement of the DCPD removal flux due to the presence of PASP as a function of pH:  $J_L$  is the removal flux for solutions containing 600 ppm PASP, and  $J_0$  is the removal flux of solutions at the same pH without PASP. Lines are smooth fits of the data.

minimum role. Note that the transition from a pH-dependent regime to a pH-independent regime occurs at a pH of approximately 5.

The addition of PASP (600 ppm) causes a significant change in the measured trends in the flux with changes in the pH (Figure 8). At  $\text{pH} \leq 4$ , the data are not significantly different from the results without PASP. The fact that the removal rate is indifferent to the presence of the sequestrant indicates that acid dissolution, rather than sequestration by PASP, is predominant at low pHs. By comparison, for pHs between 4 and 10, there is an increase in the removal rate in the presence of PASP. Even though previous research has shown that the removal mechanisms of HAP/DCPD and DCPD are qualitatively very different (surface dissolution and shear removal);<sup>13</sup> the addition of PASP in both cases leads to an increase in the removal rate.<sup>11</sup> It is interesting to note that the removal flux in the presence of PASP decreases uniformly with pH, without exhibiting the two pH regimes found in the absence of PASP.

The results in Figure 8 indicate that the effectiveness of PASP to increase removal rates at 600 ppm is optimum at intermediate pHs. To better visualize this trend, in Figure 9 we compare the ratio of the removal flux in the presence of PASP to the flux corresponding to acid dissolution as a function of pH, including results for various fluid velocities. We can see that the maximum enhancement of removal rates occurs at pH 5 for all fluid velocities. In addition, the removal flux in the presence of PASP is more than 35 times the flux without PASP at  $v = 2.4$  m/s and pH 5, which shows the effectiveness of PASP as an additive for the removal of DCPD deposits.

We have used the mathematical model developed in this work to represent the data obtained in the range of pHs and fluid velocities used in Figure 9. The adjustable parameters were selected to minimize the relative error between the model predictions and the data. Two initial constraints were imposed on the fitting parameters. First, we started by considering  $k_A = 0$  (eq 7), which means that the acid dissolution reaction is irreversible. Because a good fit of the data in the absence of PASP was obtained for this condition using  $k_R$  as the only adjustable parameter as a function of pH,  $k_A = 0$  was considered to be the final fitted value. Also, when fitting data in the presence of PASP, we considered, as an initial guess, that the equilibrium constants for complexation of calcium ions by PASP species were all the same:  $K_{\text{ME}1} = K_{\text{ME}2} = K_{\text{ME}3}$  (see Table 1); however,

**Table 2. Parameters Used To Fit the Model to the Experimental Data<sup>a</sup>**

parameter	pH	value
$k_R$ (kmol/m <sup>2</sup> ·s)	2.85	$4.5 \times 10^{-7}$
	3.50	$2.0 \times 10^{-7}$
	4.00	$1.4 \times 10^{-7}$
	4.50	$5.6 \times 10^{-8}$
	5.00	$6.3 \times 10^{-9}$
	6.00	$4.0 \times 10^{-9}$
	8.00	$3.9 \times 10^{-9}$
$k_{P1}$ (kmol/m <sup>2</sup> ·s)	10.0	$5.7 \times 10^{-9}$
	all	$4.5 \times 10^{-6}$
$k_{P2}$ (m <sup>4</sup> /kmol·s)	all	$3.0 \times 10^2$
$K_L$ (M <sup>-1</sup> )	all	$3.0 \times 10^5$
$K_{\text{ME}1}$ (M <sup>-1</sup> )	all	$1.3 \times 10^5$
$K_{\text{ME}2}$ (M <sup>-1</sup> )	all	$3.8 \times 10^4$
$K_{\text{ME}3}$ (M <sup>-1</sup> )	all	$3.8 \times 10^4$

<sup>a</sup> The acid dissolution rate constant  $k_R$  was fitted to experiments without PASP. These experiments were well fitted with no backward reaction ( $k_A = 0$ ). The rest of the parameters were fitted to data corresponding to 600 ppm PASP solutions.

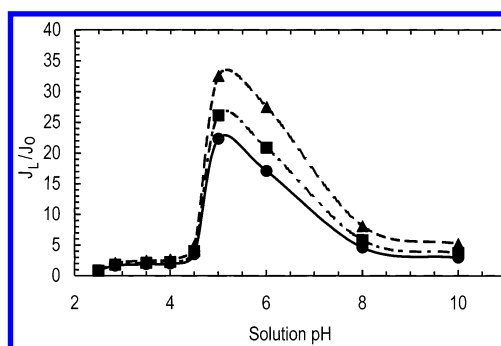


**Figure 10.** Model predictions for  $J_L/J_0$  as a function of pH. The adjustable parameters were selected to fit the data in Figure 9. The values used to generate these results are presented in Table 2. Solid lines are model predictions, and markers are included at selected points for identification purposes. The legend is as in Figure 9.

the data could not be fitted satisfactorily under these conditions. For this reason, we tried keeping  $K_{\text{ME}2} = K_{\text{ME}3}$ , but fitted a different value for  $K_{\text{ME}1}$ . A good fit of the data was obtained. In the final fit,  $K_{\text{ME}1} > K_{\text{ME}2}$ , indicating a stronger calcium complexation by the more ionized PASP species. The parameters that yield the best fit are shown in Table 2, and the predictions of the model are presented in Figure 10.

Comparing Figures 9 and 10, we can see that the model is capable of representing the trends followed by the removal flux as a function of pH and velocity. One difference between the model and the data is that the model yields a lower sensitivity of  $J_L/J_0$  on velocity: at the optimum pH (pH 5), the predicted values of  $J_L/J_0$  range between 22.5 and 33 between the lowest and highest velocities, whereas the experimental values of  $J_L/J_0$  range between 22 and 35. The effect of velocity will be discussed in more detail below.

The fact that the model proposed in this work can represent the experimental data with relative accuracy enables identification of the factors that control the shape of the curves in Figures 9 and 10. At low pHs, dissolution of DPCD from sites of the surface without PASP (acid dissolution) controls the process and hence adding PASP does not result in an appreciable enhancement of the removal flux. As the pH increases, dissolution due to PASP complexation of calcium on the surface becomes important and enhancement is observed until the optimum point, located around pH 5. It is important

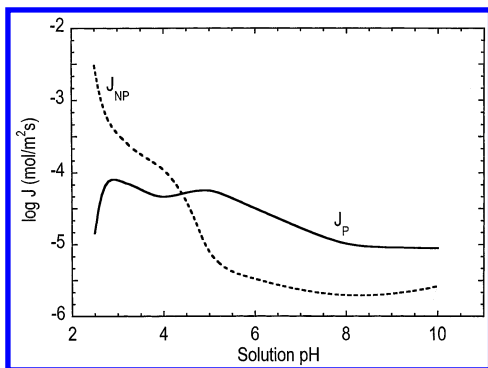


**Figure 11.** Model predictions of contributions to the removal flux from acid dissolution ( $J_{NP}$ ) and PASP complexation ( $J_P$ ) as a function of pH for  $v = 1.2$  m/s and 600 ppm PASP. Note that the acid dissolution flux follows the data for dissolution without PASP (Figure 8).

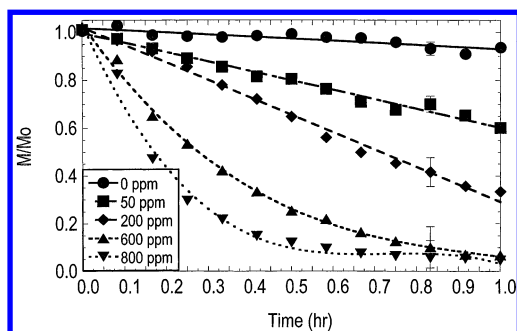


**Figure 12.** Removal of DCPD deposits from stainless steel at various PASP concentrations for pH 5 and  $v = 1.2$  m/s.

to mention that, at pH 5 and higher, the polyaspartate dissociation equilibrium (Table 1) reveals that the dissolved PASP is completely in the form of  $\text{PASP}^{4-}$ ,  $\text{HPASP}^{3-}$ , and  $\text{H}_2\text{PASP}^{2-}$ , which are the species more likely to complex with calcium. On the other hand, between pH 6 and 10, the dominant dissolved phosphate species is  $\text{HPO}_4^{2-}$ , whose presence inhibits complexation dissolution of DPCD by PASP (eq 8). Hence, this tends to diminish the impact of the effect of PASP on dissolution rates, although an improvement with respect to the absence of PASP is noted until pH 10. These trends are better illustrated by Figure 11, which shows the predicted removal fluxes  $J_P$  and  $J_{NP}$  as a function of pH. The acid dissolution flux ( $J_{NP}$ ) dominates at low pHs, but it drops rapidly between pH 2 and 5. The removal flux due to PASP complexation ( $J_P$ ) does not change dramatically over the whole range of pH but dominates over the acid dissolution flux at pHs above 5. Surface coverage by PASP ( $\theta$ ) increases monotonically between 0.1 at low pHs to 0.6 at high pHs.

The results presented demonstrate the effectiveness of PASP to enhance the removal of DCPD deposits, with an optimum enhancement at pH 5. Figure 12 shows the effect of the PASP concentration at that pH on the cleaning curves. Note how a removal of less than 10% of the film after 1 h in the absence of PASP is progressively improved until almost complete removal at 600 and 800 ppm PASP.

The effect of PASP concentration on the initial removal rate is shown in Figure 13, along with the model predictions. The model represents the trends of the experimental data with variations in the PASP concentration for pHs 5 and 8. At pH 4, the model predicts a slight enhancement of the removal rate that is not seen in the experimental data. Considering that

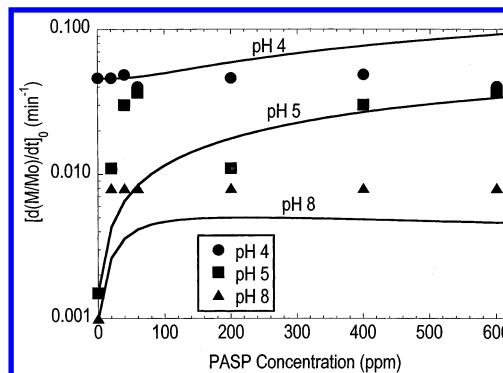


**Figure 13.** Initial removal rates as a function of PASP concentration for various pHs and  $v = 1.2$  m/s. The lines represent model predictions.

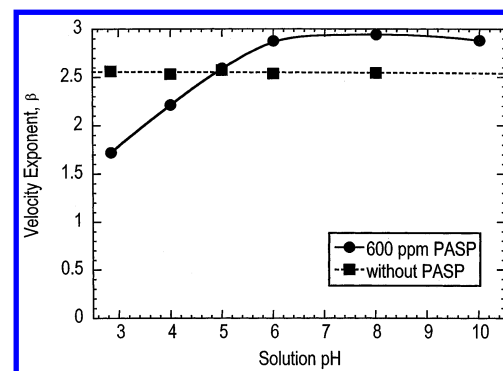


**Figure 14.** Velocity exponent for DCPD removal with 600 ppm PASP and without PASP. Lines are smooth fits of the data.

the parameters used in the model calculations were fitted to data at 600 ppm PASP (Table 2), plus the fact that the model only deals with dissolution and mass transfer and not shear removal (see below), the comparison between model and data trends confirms the validity of the mechanisms proposed.

We also explored the effect of fluid velocity on removal rates. As indicated above (Figure 3 and associated discussion), the exponent of the relation between the removal flux and the average velocity gives an indication of the prevailing removal mechanism. The initial removal fluxes at fixed pH and PASP concentrations have been fitted to the average velocity, using the equation

$$J \propto v^\beta \quad (13)$$

Values obtained for the exponent are shown in Figure 14 for removal in the absence of PASP and with a PASP concentration of 600 ppm. Recall that  $\beta = 0$  for dissolution-limited removal,  $\beta = 0.83$  for mass-transfer-limited removal, and  $\beta = 2$  for shear removal. In the absence of PASP, the high value of the exponent indicates that removal is predominantly due to detachment of particles from the deposit under the action of shear forces. In addition, the fact that the exponent does not change with pH indicates that, even though removal rates change, the mechanism remains invariant. In the presence of PASP, the exponent tends to decrease at low pHs, indicating that mass transfer or the kinetics of the dissolution process at the surface are starting to play a role as removal mechanisms. However, the value of the exponent is relatively high in the whole range of pHs, which suggests that shear is the predominant removal mechanism.

## Conclusions

A study of the removal mechanisms of DCPD in the presence of PASP suggests that DCPD removal is controlled by shear and influenced by the interfacial dissolution process. The presence of PASP enhances the removal rate by increasing the rate of the interfacial dissolution processes occurring at the solid surface. Presumably, local dissolution rates produce a decrease in the adhesion forces between solid particles and the rest of the film, thereby allowing removal by shear forces. The most dramatic improvement in removal rates due to PASP occurs at pH 5. The effect of local dissolution rates is confirmed by the fact that the model developed in this work, which considers only dissolution reactions and mass transfer, can reproduce the trends observed in the experimental data.

Overall, the removal of DCPD remains dominated by shear even in the presence of PASP. Although the rate-controlling mechanism is unchanged, the presence of PASP enhances DCPD removal over a wide range of pHs by calcium sequestration. The optimal PASP performance at pH 5 provides opportunities to remove mineral deposits under conditions that are not excessively acidic (which may cause metal corrosion) or alkaline (which may cause salt precipitation).

## Acknowledgment

We gratefully acknowledge support by the National Science Foundation (Grant CTS-9500399 and 9616638). We acknowledge the Nuclear Engineering Department at North Carolina State University (Pedro Perez, Jack Weaver, and Jerry Wicks) for supplying the radiolabeled calcium phosphate for the solid scintillation cleaning studies and Kit Yeung for his assistance in setting up the experimental flow apparatus. Additionally, the use of SEM facilities at the Center for Interfacial Engineering of the University of Minnesota is appreciated. We would like to thank Rohm and Haas for providing the PASP.

## Literature Cited

- (1) Amjad, Z. Development of Calcium Phosphate Inhibiting Polymers for Cooling Water Applications. In *Calcium Phosphate in Biological and Industrial Systems*; Amjad, Z., Ed.; Kluwer Academic Publishers: Boston, 1998; p 371.
- (2) Cahn, A. Builder Systems in Detergent Formulations. *Int. News Fats Oils Relat. Mater.* **1994**, *5*, 70.
- (3) Means, J. L.; Kucak, T.; Crerar, D. A. Relative Degradation Rates of NTA, EDTA and DTPA and Environmental Implications. *Environ. Pollut., Ser. B* **1980**, *1*, 45.

- (4) Xue, H.; Sigg, L.; Kari, F. Speciation of EDTA in Natural Waters: Exchange Kinetics of Fe-EDTA in River Water. *Environ. Sci. Technol.* **1995**, *29*, 59.
- (5) Garris, J. P.; Sikes, C. S. Use of Polyamino Acid Analogues of Biomineral Proteins in Dispersion of Inorganic Particulates Important to Water Treatment. *Colloids Surf. A* **1993**, *80*, 103.
- (6) Nakato, T.; Yoshitake, M.; Matsubara, K.; Tomida, M. Relationships Between Structure and Properties of Poly(aspartic acid). *Macromolecules* **1998**, *31*, 2107.
- (7) Freeman, M. B.; Paik, Y. H.; Wilczynski, R.; Wolk, S. K.; Yocom, K. M. Biodegradability of Polycarboxylates: Structure-Activity Studies. In *Hydrogels and Biodegradable Polymers for Bioapplications*; Ottenbrite, R. M., Huang, S. J., Park, K., Eds.; American Chemical Society: Washington, DC, 1996.
- (8) Sikes, C. S.; Wheeler, A. P. Regulators of Biomineralization. *Chem. Technol.* **1988**, 620.
- (9) Mueller, E.; Sikes, C. S. Adsorption and Modification of Calcium Salt Crystal Growth by Anionic Peptides and Spermine. *Calcif. Tissues Int.* **1993**, *52*, 34.
- (10) Silverman, D. C.; Kalota, D. J.; Stover, F. S. Effect of pH on Corrosion Inhibition of Steel by Polyaspartic Acid. *Corrosion* **1995**, *51*, 818.
- (11) Littlejohn, F.; Sáez, A. E.; Grant, C. S. The Use of Sodium Polyaspartate in the Removal of Hydroxyapatite/Brushite Deposits from Stainless Steel Tubing. *Ind. Eng. Chem. Res.* **1998**, *37*, 2691.
- (12) Christoffersen, J.; Christoffersen, M. R. Dissolution of Calcium Hydroxylapatite and its Applications to Biological Demineralization. *Croat. Chem. Acta* **1983**, *56*, 769.
- (13) Littlejohn, F.; Sáez, A. E.; Grant, C. S. Mechanisms for the Removal of Calcium Phosphate Deposits in Turbulent Flow. *Ind. Eng. Chem. Res.* **2000**, *39*, 933.
- (14) Grant, C. S.; Webb, G. E.; Jeon, Y. W. Calcium Phosphate Decontamination of Stainless Steel Surfaces. *AIChE J.* **1996**, *42*, 861.
- (15) Grant, C. S.; Webb, G. E.; Jeon, Y. W. A Noninvasive Study of Milk Cleaning Processes: Calcium Phosphate Removal. *J. Food Process Eng.* **1997**, *20*, 197.
- (16) Yan, J.; Sáez, A. E.; Grant, C. S. Removal of Oil Films from Stainless Steel Tubes. *AIChE J.* **1997**, *43*, 251.
- (17) Kabin, J. A.; Sáez, A. E.; Grant, C. S.; Carbonell, R. G. Removal of Organic Films from Rotating Disks Using Aqueous Solutions of Nonionic Surfactants: Film Morphology and Cleaning Mechanisms. *Ind. Eng. Chem. Res.* **1996**, *35*, 4513.
- (18) Cleaver, J. W.; Yates, B. Mechanism of Detachment of Colloidal Particles from a Flat Substrate in Turbulent Flow. *J. Colloid Interface Sci.* **1973**, *44*, 464.
- (19) Welty, J. R.; Wicks, C. E.; Wilson, R. E. *Fundamentals of Momentum, Heat, and Mass Transfer*; Wiley: New York, 1984.
- (20) Lindsay, W. L. *Chemical Equilibria in Soils*; Wiley: New York, 1979.
- (21) Littlejohn, F. The Effect of Poly(Aspartic Acid) on the Removal Rates of Brushite Deposits from Stainless Steel Tubing in Turbulent Flow. Ph.D. Dissertation, North Carolina State University, Raleigh, NC, 1999.

Received for review February 4, 2002  
 Revised manuscript received June 13, 2002  
 Accepted June 24, 2002

IE0201011